Developing a test procedure for neutron detection/non detection using a Small TPC Prototype

Bachelor thesis
autumn 2015, 15 ECTS
by Nicholai Mauritzson

Supervisor: Anders Oskarsson
Department of Particle Physics
Lund University

January 20, 2016

LUND UNIVERSITY

Abstract

This work relates to the proposed $n - \bar{n}$ experiment at ESS and covers a procedure with which future neutron research can be made using a small TPC prototype. Settings for the GEM amplification voltage supply and main drift field across the chamber have been established using minimum ionizing cosmic muons as a reference. To be able to reconstruct tracks in three dimensions and measure the deposited energy of a particle, a track-finding and plotting software was also designed as part of this work. From measurements with an AmBe source a preliminary detection efficiency for gammas and thermal neutrons has been established. Future improvements regarding work with the small TPC prototype are suggested in terms of the pad size and geometry, improving the efficiency measurements and track-finding.

Contents

List of abbreviations

- TPC - Time Projection Chamber
- TPCp - Small TPC Prototype
- ESS - European Spallation Source
- MIP - Minimum Ionizing Particle
- FEC - Front End Card
- RCU - Readout Control Unit
- ADC - Analogue to Digital Converter
- PCA - Programmable Charge Amplifier
- YAP:Ce - Yttrium Aluminium Perovskite activated by Cerium (gamma detector)
- AmBe - Americium-241 and Beryllium-9
- PMT - Photomultiplier Tube

1 Introduction

During the development of the European Spallation Source (ESS) [1] it is logical to foresee a need to study the response of different tracking and calorimeter detectors for fast and thermal neutrons. This thesis aims to take the first steps towards establishing a test procedure using neutrons from neutron sources, based on radioactive decay, with the Small Time Projection Chamber Prototype (TPCp) at the Division of Particle Physics at Lund University. A TPC is one of the intended methods of tracking for the proposed $n-\bar{n}$ experiment at ESS [8]. The radioactive sources are made available by the Detector Group of the European Spallation Source and the Source-based Neutron Irradiation Group of the Division of Nuclear Physics (SoNnIG) at Lund University.

1.1 ESS and the $n - \bar{n}$ experiment

The European spallation source (ESS), planned for 2019, is in the foreseeable future slated to be the worlds highest intensity neutron source. Using a linear accelerator, protons will be accelerated towards a target consisting of a neutron rich material, like tungsten, and neutrons are emitted through the process of spallation. The neutrons are collected and moderated before ending up at various research stations around the perimeter. ESS will host research in many fields including, medicine, material science and chemistry.

With such a high intensity of neutrons, ESS is also of interest to the field of particle physics with the proposal to build an experiment which aims to observe the oscillation from a neutron to an anti-neutron ($n - \bar{n}$). According to the standard model of particle physics (SM), the earliest universe contained equal amounts of matter and antimatter, which comes from the conservation of baryon number (B). Today we observe only matter, which implies that there is some mechanism which breaks this expected symmetry. Being a baryon, the transformation of a neutron ($B = 1$) to an anti-neutron ($B = -1$) would allow a symmetry breaking of $\Delta B = 2$.

The proposed experiment uses 10^{13} thermal neutrons per second travelling with an average velocity of 800 m/s along a 200 m beam line in vacuum. After a neutron has oscillated into an anti-neutron it needs to undergo annihilation in order to be detected. This needs to happen in a controlled manner so that the annihilation occurs within the boundaries of the detector. This can be done by having the anti-neutrons pass through a thin target (0.2 mm carbon foil, for example) in which all anti neutrons annihilate. An annihilation is expected to produce various configuration of pions (π). Eq. 1 shows the most prominent reaction channel with a branching ratio of 28% [5]. The charged pions can be tracked in a tracking detector, like a time projection chamber, while the neutral pions are detected in the electromagnetic calorimeters.

$$n + \bar{n} \rightarrow \pi^+ + \pi^- + 3\pi^0 \tag{1}$$

A sketch of the proposed $n-\bar{n}$ experiment is shown in figure 1. The figure shows the beam line, location of annihilation target and the tracker, and calorimeters, which encompass the beam tube.

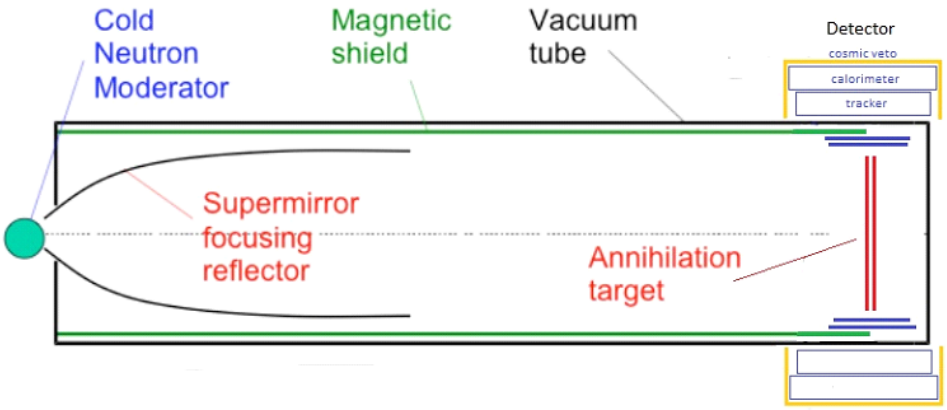

Figure 1: Schematic view of the proposed 200 m long beam line for the $n - \bar{n}$ experiment at ESS. The diameter is 2 m, and located in the center of the detector system is the annihilation target. Dimensions are not to scale, and the final design of the experimental set-up is not yet done [19].

Detecting these annihilation products is a fairly straightforward concept. The deposited energy is equivalent to two neutron masses ($\approx$ 1.88 GeV) compared with the expected background events which have much lower energy.

A significant amount of thermal neutrons is expected to scatter off the annihilation target or walls of the beam line and make it into the detector, a process which through secondary events is expected to create many additional ionization readings. This may create an excessive counting rate for the individual readout channels, potentially "hiding" the annihilation event. To discriminate against events associated with cosmic rays, the detector set-up is enclosed in scintillators with logic to discriminate against these events.

By virtue of being free neutrons, spontaneous decay during the time they drift from the spallation target to the detectors will occur. Free neutrons have a mean life of about 14.6 minutes, so with an initial rate of 10^{13} neutron per second, it is expected that around 10^8 neutrons will decay within the length of the detector. Eq. 2 shows the products from the free neutrons beta-decay.

$$n \rightarrow p + e^- + \bar{\nu}_e \tag{2}$$

The emitted electrons will further increase the background of the experiment, while the protons will be stopped in the walls of the beam tube due to their low energy.

One immediate goal of this work is to study the probability that thermal neutrons entering the gaseous tracker, in this case a TPC, will make a detectable ionization event, which will constitute background for the measurement.

1.2 Particle interaction with matter

A particle is detected due to its interaction with the material of the detector. This might be, although very unlikely, the short-range interaction by the weak force, or more probable (if the particle is a hadron) through the strong force. A third method of interaction is the long-range electromagnetic force, which applies to charged particles. The two latter will be the focus of this report. A consequence of the electromagnetic interaction is that charged particles will ionize atoms as they interact with them, "freeing" electrons from the atom. This property is the central working mechanism for detecting charged particles with gas-detectors, such as a TPC.

1.2.1 Charged particle interaction with matter

As a charged particle interacts with matter, it loses energy, per unit length, depending on the atomic number and atomic mass number of the material (Z and A), the velocity of the particle (β) and the charge of the particle (z). The dominant dependence is given in Eq. 3 and is an approximated version of the Bethe-Bloch equation [18].

$$\frac{dE}{dx} \propto \frac{Z \cdot z^2}{A \cdot \beta^2} [\, \cdots \,] \tag{3}$$

The inverse relation to the velocity comes from the fact that at lower velocities the particle will have "more time" to interact with an atom, transmitting more of its energy to it. Figure 2 shows the results of measurements taken for the deposited energy as a function of the particle momentum in a TPC. It clearly illustrates the velocity dependence from Eq. 3 where, for a given momentum, the more massive particles deposit more energy per centimetre due to lower velocity. The increased dE/dx at higher momentum are due to relativistic effects, known as the "relativistic rise", which have been left out of Eq. 3.

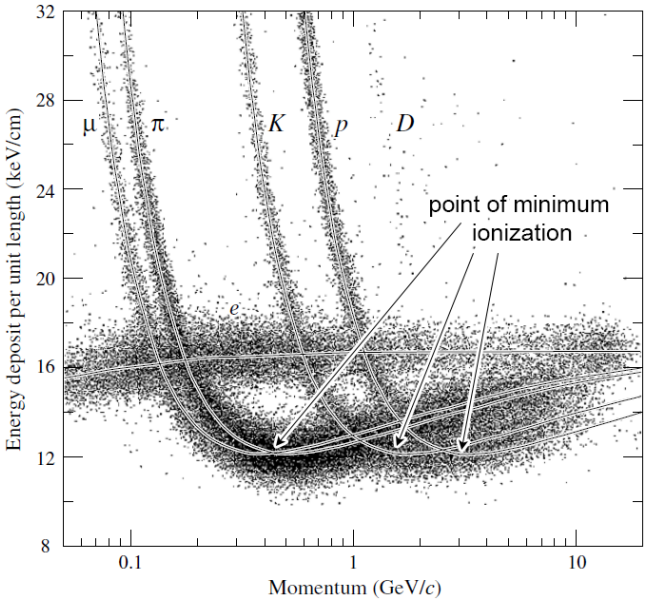

Figure 2: Deposited energy [keV/cm] for several different singly charged particles as a function of momentum. Measurements taken in Ar-CH_4 (80:20) at 8.5 atm. The points of minimum ionization for the different particles are marked in the figure [11].

All particles have a region of "minimum ionization" energy, where the amount of energy loss per unit length is at its minimum ($\beta \approx 1$). With a velocity near the speed of light, the cosmic muon momentum is mainly in this regime, and cosmic muons therefore can be regarded as minimum ionizing particles (MIPs). As seen from the Bethe-Bloch formula Eq. 3, the minimum dE/dx is obtained as $v \to c$. Cosmic muons are of course readily available, and by using tabulated data of their ionization in a specific material [20] it is possible to calibrate detectors for energy loss. This method is used in section 3.2.

1.2.2 Photon interaction with matter

Photons interact electromagnetically with matter in three principle ways.

- Photoelectric effect; where the absorption of the photon causes the emission of an electron which carries almost the full photon energy.
- Compton scattering; where the photon transmits a certain portion of its energy to an electron and scatters, changing direction. This allows for a wider range of energies to be imparted to the emitted electron.
- Pair production; where the photon creates an electron and positron pair, will occur in the vicinity of the electric field of a nucleus, and the energy of the photon must be at least two times the electron rest mass (1.022 MeV).

The probability for each of these interactions to occur is dependent on the photon energy. As an example, the photon cross-section for different processes in lead is shown in figure 3.

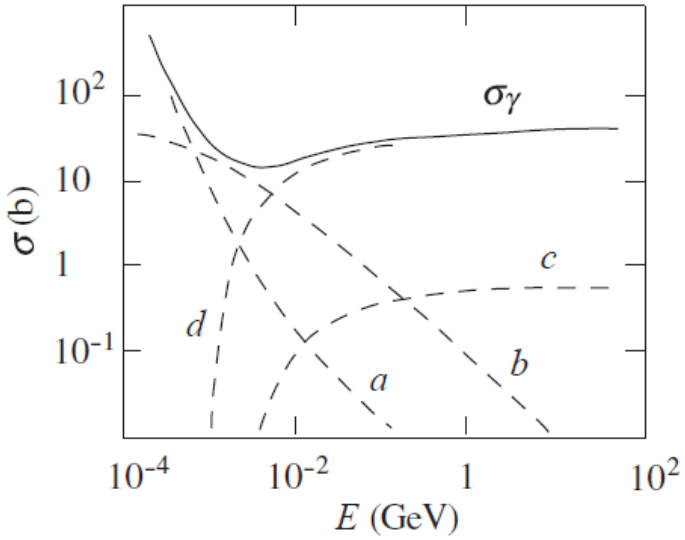

Figure 3: Probability of interaction of a photon in lead as a function of energy. σ_γ is the total photon interaction cross-section composed by, a photoelectric effect, b Compton scattering, c pair production in the field of the atomic electrons, d pair production in the field of the atomic nucleus. [16]

The photon interaction cross section depends strongly on the atomic number of the material (Z). At typical nuclear physics energies of a few MeV, the probability for photoelectric effect is proportional to Z^5, while Compton scattering is proportional to Z [19].

1.3 Time Projection Chamber

A Time Projection Chamber (TPC) is a type of gas detector which is able to reproduce a three-dimensional image of the charged particle track, as well as to measure the deposited energy (dE/dx) due to ionization. When used in conjunction with an externally applied magnetic field, the particle's momentum can also be determined. The TPC contains a gas mixture like argon and carbon dioxide (Ar-CO_2), which gets ionized along the particle path as the incident charged particle travels through it. An applied potential across the chamber will separate and accelerate the electrons and ions which are produced in the ionization process. The electrons and ions drift anti-parallel to each other across the

chamber until they reach the anode and cathode, respectively. The ionisation electrons will distribute their charge at the anode plane and be sampled by the TPCs readout system. For a more detailed description of a typical electronic readout system see section 2.1.

Figure 4 shows a schematic overview of the ionisation and drift process in a TPC. The position where the electrons hit the anode plane gives the position in two dimensions (x,y), while the time it takes for the electrons to reach it gives the third dimension (z). This time projection is achieved by knowing the average drift velocity of the electrons, which is given by the electric field, as well as composition and pressure of the gas [20].

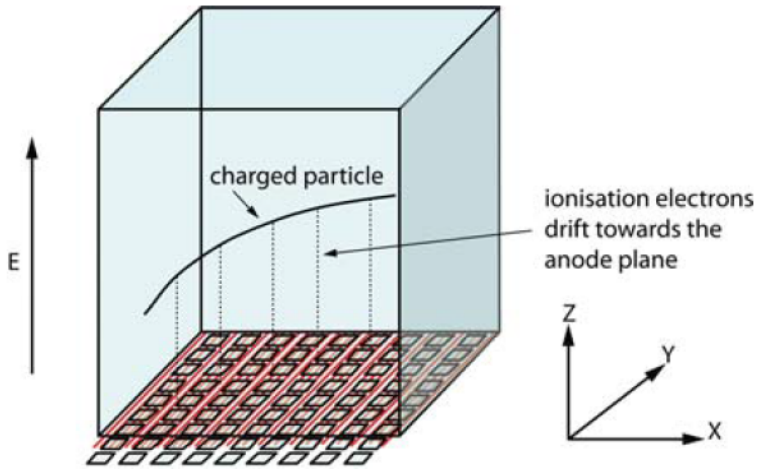

Figure 4: Principles of a TPC schematically represented using a simple box. The electron's drift time gives a position along the z-axis, and the impact position on the anode plane gives the x and y coordinates. [21]

1.3.1 Amplification

Even though a charged particle is able to produce numerous electrons through the ionization with the gas, as they reach the anode plane of the TPC, the signal they produce is way below the electronic noise threshold of the readout electronics. In other words, the signal can not be resolved. To overcome this problem there is a need for an amplification of the signal before it reaches the anode plane. Normally this is achieved by using either anode wires (in the form of a multi wire proportional chamber, MWPC) or gas electron multipliers (GEMs). Both work on the principle of avalanche multiplication in a strong electric field. This accelerates the electrons, giving them enough energy to ionize the gas further and creates an exponentially increasing avalanche effect. An amplification factor of several thousand can then be produced in this way, while still maintaining the proportionality to the deposited energy. A setback of this amplification process is that the ionization which the electrons achieve also excites the atoms in the gas. The de-excitation then gives rise to a large number of photons, which might cause further ionization, in particular when hitting metallic surfaces, and produce further amplification, which may escalate to a discharge. The presence of an "absorber" in the gas mixture, like CO_2, solves this by absorbing these photons without further ionization.

Amplification by anode wires: The anode wire plane consists of thin wires, over which a positive potential is applied. As the drifting electrons approach the anode wire, the effective electric field will increase, proportionally to $1/R$, where R is the distance to the wire, until reaching a maximum just before they hit the wire. This creates, dependent

on the gas mixture and pressure, a massive amplification. The signal is read out on the segmented wire chamber cathode.

Amplification by GEMs: GEMs work by creating a high E-field through which the electrons will pass over a very small distance, typically in the range of 50μm. Figure 5 shows a schematic view of the GEMs used in this report with the size of the holes and pitch noted. The GEM is constructed as a foil with a conductive surface on the top and bottom, which correspond to the cathode and anode of the GEM foil. The conductive surfaces are separated by a layer of kapton.

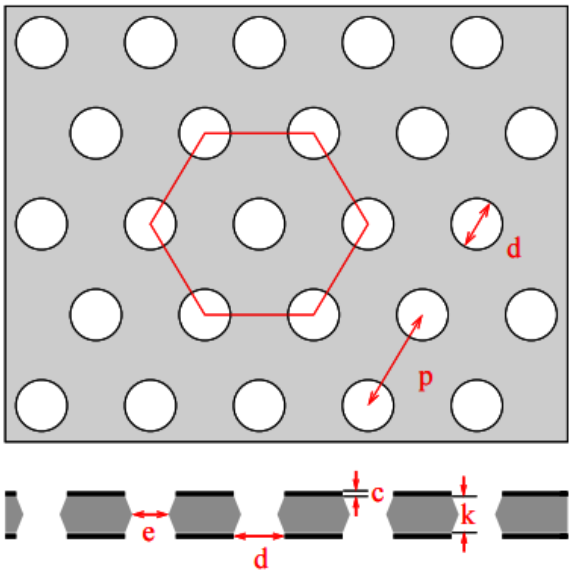

Figure 5: Schematic view of the GEM used as part of this project. Inner hole diameter is $e = 50 \pm 5\mu$m, diameter is $d = 70 \pm 5\mu$m, pitch is $p = 140\mu$m, thickness of copper coating is $c = 5\mu$m and the kapton thickness is $k = 50\mu$m. [15]

With a distance separation of 50μm and using an effective potential difference of 340V (see section 3.1) a GEM will produce a 68 kV/cm electric field (Eq. 4) in each of its holes.

$$E = \frac{340\text{V}}{50\mu\text{m}} = 6.8\text{V}/\mu\text{m} = 68\text{kV/cm} \tag{4}$$

Figure 6 shows a simulation of the electric field lines and equipotential lines for two of the holes in a GEM.

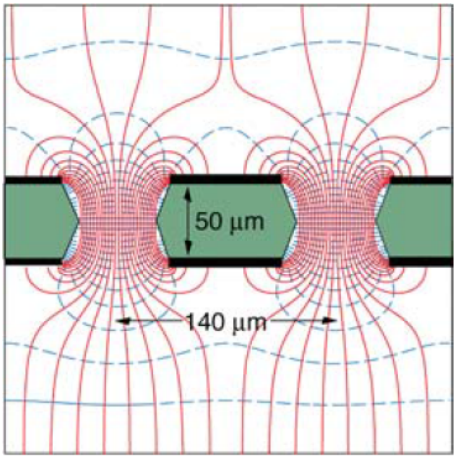

Figure 6: Simulation of field lines (solid lines) produced for two of the holes on a GEM. Dashed lines represent the equipotential surfaces [21].

GEMs can be constructed using advanced photo lithographic methods, which are similar to the manufacturing of printed circuit boards. Normally, several GEMs are stacked in order to achieve an amplification of a factor of thousands. The experiments performed for this report utilize three layers of GEMs for amplification.

1.3.2 Diffusion and pad readout

As the electrons drift across the chamber and hit the anode plane of the detector, there is an uncertainty in the position, since the electrons "diffuse" by interactions in the gas when they drift through the chamber. This means, essentially, that they hit a larger portion of the anode plane which, when looking at the track reconstruction, shows up as "wider" tracks. This is also indicative of a highly ionizing particle since, for a given GEM amplification, more ionization electrons means that there is more diffusion which gives a signal over the threshold and produces an even wider track. This is not really a problem since a wider track allows for a better determination of the coordinates of the track by charge sharing. Adjacent pads will then obtain a signal, and calculating a mean value will produce a position measurement with an accuracy which is better than the pad sizes. However, the anode plane needs to be designed with the direction of the particles trajectories in mind. Figure 7 shows a good and a bad configuration, in the case of a GEM and padplane set-up, for the projection of two tracks from different directions. The left figure clearly gives a superior resolution, while the right one would only produce a straight line upon reconstruction.

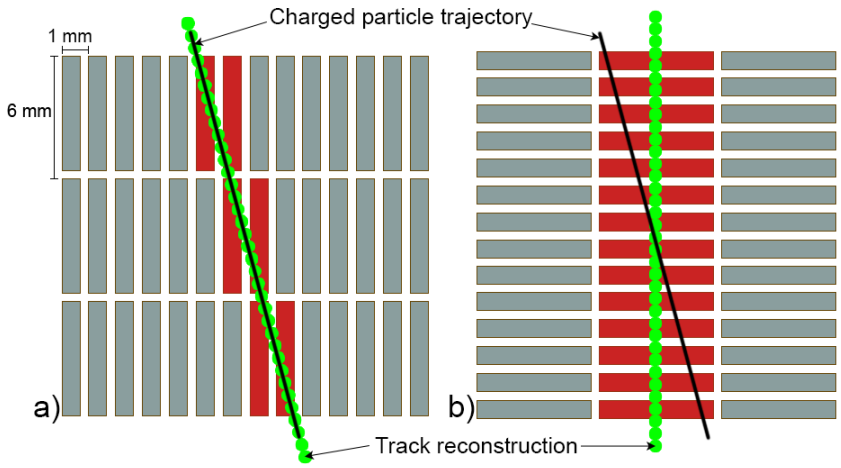

Figure 7: A representation of the padplane and how, depending on its geometry, the direction of the incoming particle influences the spatial resolution which can be obtained. A red color indicates pads which have received signals over threshold from the ionization. Black line is the trajectory of the charged particle, and the dotted green line is the reconstructed path. Rectangular pads like these are adequate when there is a pre-defined direction for the particles. Schematic view shows 42 channels.

Obviously, smaller pads provide a better spatial resolution for the tracks, and a symmetrically designed pad (a square, for example) would make the system more independent of the direction of the tracks. The reality is that the electronic readout systems have a limit to how many pads it is possible to connect to for a given area, so some compromises need to be made. The pad shape used in these experiments is rectangular, as it was designed for track directions like in figure 7a. However, for the experiments performed as part of this report, there is no preferred direction, which means that the track information can not be read out with optimal pad geometry.

1.3.3 Re-absorption of electrons in the gas

Before a gas detector, such as a TPC, can be put into operation, it needs to have its gas volume replaced with the operating gas several times. This is to avoid any presence of oxygen and water molecules, which have very high attachment cross-section for electrons. These molecules would absorb electrons and thus prevent them from reaching the anode plane. Those which still make it will not accurately represent the ionization which had occurred in the chamber. Usually, several days are required to flow gas through a TPC of a significant size, and once the TPC is not in use, it is customary to continuously flush the system with a less expensive inert gas like N_2 to keep it free from atmospheric contaminants. The pressure is kept at slightly above atmospheric pressure to avoid leakage or back-flow.

2 The Small TPC Prototype

The Small TPC Prototype (TPCp) at Lund University's division of Particle Physics utilizes a modified version of the the readout electronics from the ALICE experiment at CERN. This modification was originally designed for the Large TPC Prototype at DESY for research relating to the future International Linear Collider experiment, and entails

the addition of the PCA16 chip to the Front End Cards (FECs). This is further discussed in section 2.1.

Other than the obvious size difference, the TPCp set-up does not have an external magnetic field. A major difference is that the TPCp does not have a beam line running through the middle of the chamber. Radiation is instead introduced from the outside of the chamber.

Figure 8 shows a schematic view of the material compositions of the TPC walls. The copper strips at the bottom are part of the field cage, and above are four layers of 0.125 mm thick Kapton bonded with an epoxy resin. The honeycomb construction is a made of a synthetic fibre material called aramid with a thickness of 5 mm. Bonded on top is a 0.25 mm thick layer of glass fibre reinforced plastic (GRP), which together with the aramid makes up the structural support of the cylindrical TPC [13].

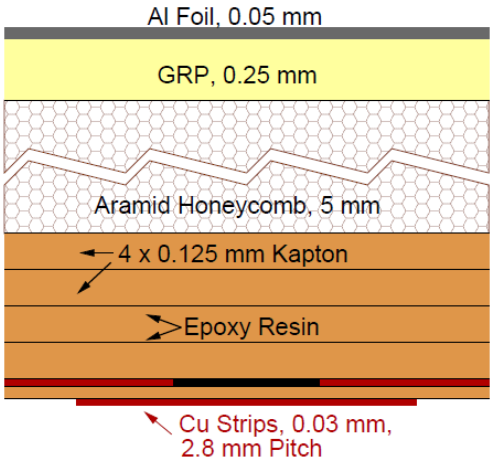

Figure 8: Schematic cross section of the wall of the TPC [13].

The Al foil is connected to ground potential in order to shield the electric field from influence by external electrical systems. One of the benefits of having a smaller chamber is that the gas used in the system can be much faster exchanged for different types and mixtures to suit the experiment. The gas inside the chamber is kept at a couple of millibars above atmospheric pressure in order to prevent regular air from leaking into the chamber. This slight excess in pressure is achieved by piping the outflow of gas through the bottom of a small container of oil.

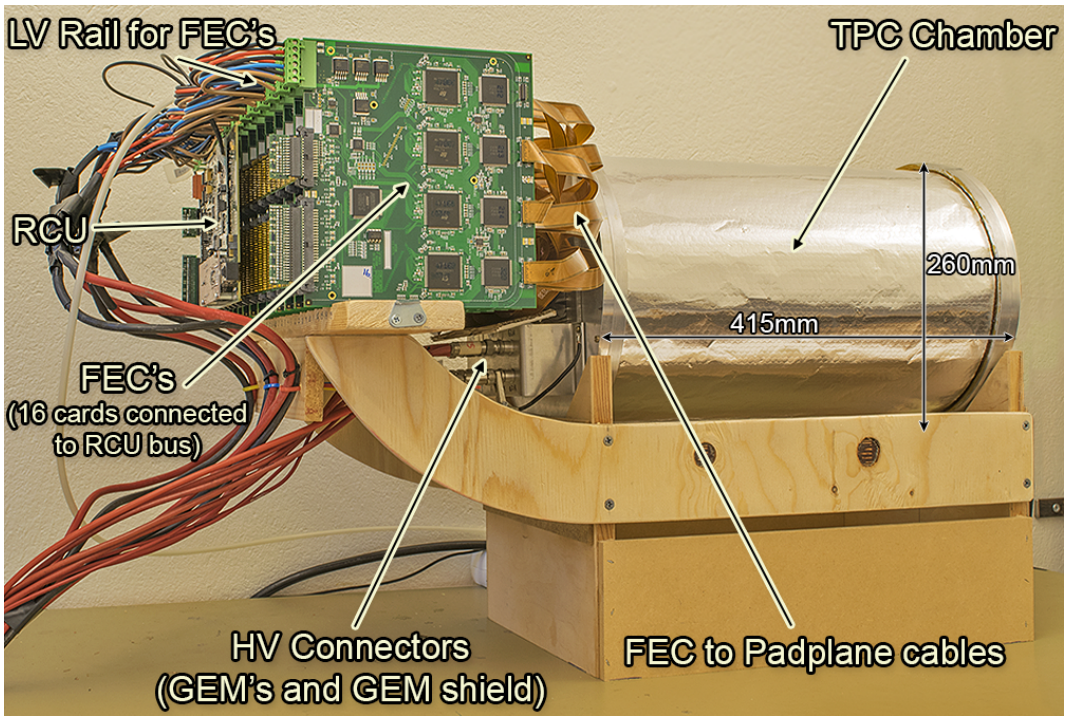

Figure 9: A picture of the TPCp which was used for this project with the various components highlighted. Photograph by author.

Figure 9 shows the arrangement of the different components that make up the TPCp. The entire set-up is mounted to a wooden base with 16 Front End Cards (FECs) mounted on top of a shelf. These are connected to the Readout Control Unit (RCU) via a bus at the back of the cards. Figure 9 also highlights the low voltage connectors for the FECs and high voltage connectors for the GEMs. The high voltage for the main drift volume is connected at the back of the chamber and is not visible in the figure. The TPCp has a flange diameter of 26.0 cm, a chamber diameter of 24.2 cm, and is 41.5 cm long with a detectable drift volume of 10x10x26.3 cm^3.

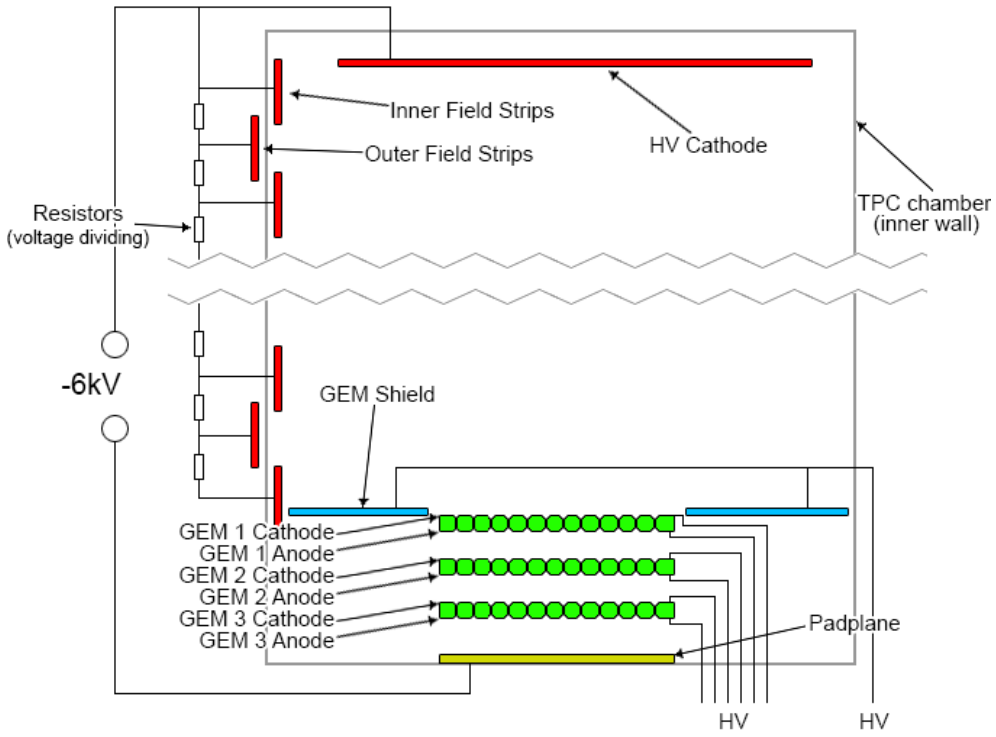

Figure 10: A schematic overview and simplified wiring diagram of the inside of the TPCp with the different components highlighted.

The inner and outer field strips along with the high voltage cathode, seen in figure 10, make up what is known as the field cage. Its purpose is to create the electric field which enables electrons to drift across the chamber to the padplane. The padplane is at ground potential of the field cage circuit. Pictures of the field strips and padplane can be seen in figure 11. Resistors are used to divide the voltage across the field strips going from the cathode to anode (padplane). The field strips keep the electric field homogeneous throughout the chamber, and their overlapping pattern allow them to cover the entire drift volume of the chamber. This field cage design is similar to the one used for the Large TPC Prototype at DESY [7]. The maximum drift distance is 26.3 cm, which equates to an average drift velocity of 0.75 cm/μs at 6000 V and atmospheric pressure with Ar-CO_2 (80:20) [10].

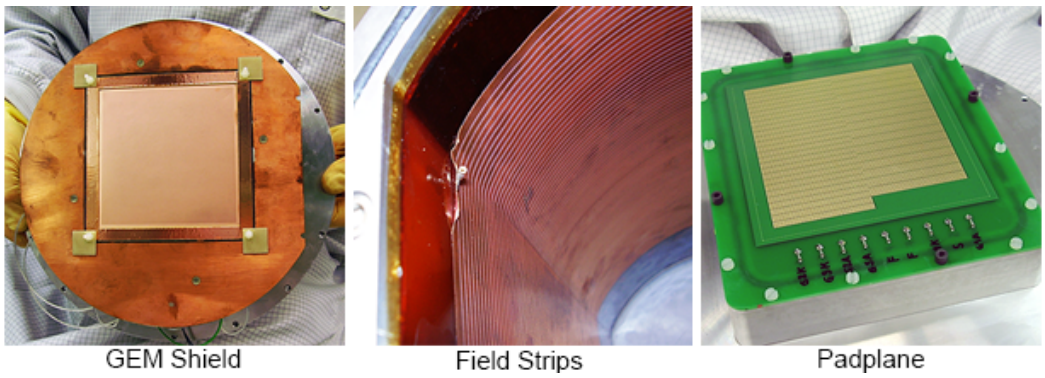

Figure 11: Pictures of the GEM shield, field strips inside the field cage and the padplane [2].

The GEM shield seen in figure 10 and 11 is a conductive plate which extends to the

walls of the drift chamber and is kept at the same potential as the cathode of GEM 1. Without the shield, the electric field would no longer be parallel to the chamber and the trajectories of the drifting electrons would be affected as they reach the first GEM plane. This would effectively ruin the drift time and projected position measurements.

Lastly, the set-up contains three GEM planes (see section 1.3.1) which E-fields can be individually modified to reach the desired amplification at the padplane.

2.1 Data acquisition and electronics

The data acquisition and electronics system used with the TPCp is made up of several components. Figure 12 shows a schematic overview of these systems. This section is divided up in to three parts covering the three major components of the system. The Front End Cards (FECs), Readout Control Unit and the computer with the communication software.

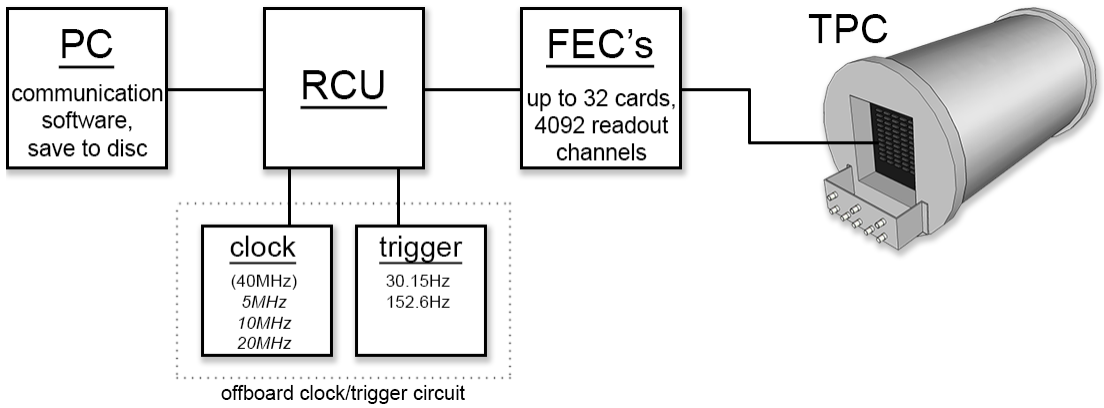

Figure 12: Schematic overview of the major components for the TPCp.

Each FEC contains 8 Programmable Charge Amplifiers (PCA16) and 8 ALTRO (ALICE TPC Read Out) chips [4]. The PCA16 first converts the charge signal from the electrons to a voltage signal, which then via the Analogue to Digital Converter (ADC) in the ALTRO gets converted to digital values. Furthermore, the PCA16 has a built in function which enables it to shape the signal for different rise time, decay time, gain and polarity [12] [17]. By being able to change the polarity of the incoming signal, the PCA16 will work for both GEMs and wire chambers which utilize negative charge signal and positive charge signal, respectively. Each PCA16/ALTRO pair is able to handle 16 channels, giving a FEC a capacity of 128 channels in total.

The RCU is the main "brain" of the system and it is with this that the computer communicates. The RCU is supplemented by a clock circuit running at 40 MHz as well as a trigger to start the recording of data. The RCU can be programmed to run at either 5, 10 or 20 MHz sampling frequency and will sample up to 1000 samples based on user choice input. The sampling frequency is the rate at which the ADC in the ALTRO will measure the voltage. These settings together with the trigger frequency will effectively decide what portion of time the system records. This will be referred to as the TPC's "time coverage" and is shown in table 3 for different trigger frequencies. For example, a 20 minute measurement with a 50% time coverage would only effectively record data for 10 minutes.

Normally a system like this is triggered with a charged particle passing the chamber, followed by sampling of voltage values. For the measurements performed here of gammas

and neutrons, no such external trigger is possible, so the system is set to arbitrarily (by a pulse generator) record a fraction of each second for analysis.

Table 1: Time coverage as a function of sampling frequency, number of samples taken and trigger frequency. The time coverage is shown as a percentage of time.

Sampl. freq.	Samples	Trigger	Time coverage
20 MHz (50 ns)	999	38.15 Hz	$\approx 0.19\%$
10 MHz (100 ns)	999	38.15 Hz	$\approx 0.38\%$
5 MHz (200 ns)	999	38.15 Hz	$\approx 0.76\%$
20 MHz (50 ns)	999	152.6 Hz	$\approx 0.76\%$
10 MHz (100 ns)	999	152.6 Hz	$\approx 1.52\%$
5 MHz (200 ns)	999	152.6 Hz	$\approx 3.04\%$

While running the measurements with the TPCp, it is of course advantageous to cover as much time as possible, especially since it is not known at what point in time an interaction will occur. Since the sampling is arbitrary in relation to the ionizing particle, the z-coordinate position does not represent the true position relative to the padplane. However, within an event and relative to each other, the track z-coordinates are correct.

The logical choice would be to choose the lowest sampling frequency that the RCU can manage and run as many samples as possible. As seen in table 3, the largest time coverage is achieved at 5 MHz sampling frequency and 999 samples (not dependent on the trigger). However, with such a low sampling rate, there is a risk of not being able to capture the entire pulse and therefore missing an event or parts of it. Taking this into account, a sampling frequency of either 10 or 20 MHz was used for measurements included in this report.

Figure 13 shows a typical pulse recorded by the ADC as it evolves over time. The ADC's sampling is analogous with that of a digital oscilloscope. The time-axis in figure 13 is calibrated with regards to the start of the pulse. Normally, after triggering, the ADC records a given number of samples at the given sampling frequency but subsequent formatting will remove the zero-values before and after the pulse to reduce data volume.

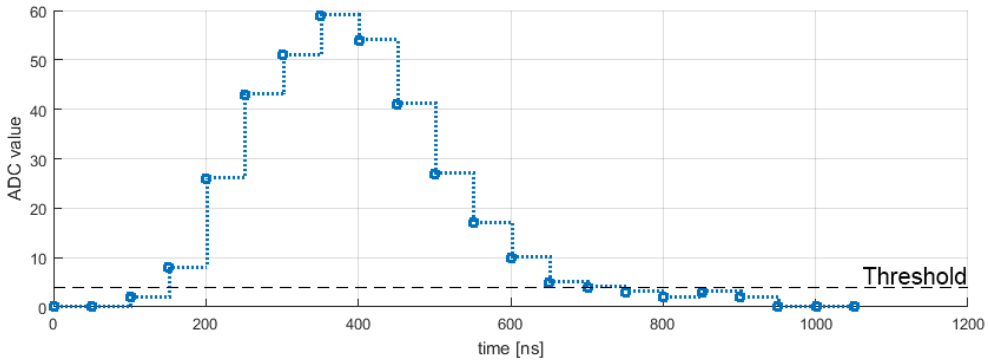

Figure 13: A typical pulse from the ADC as a function of time. The pulse in the figure was recorded using 20 MHz sampling frequency. PCA16 has a shaping time of 120 ns and amplification of 12 mV/fC. Pre-samples: 3, post-samples: 7 and the zero suppression threshold is set to 4 ADC units. The pulse is taken from measurements while measuring at cosmic radiation (see section 3.2).

The final major component of the set-up (figure 12) is the computer, which runs the

communication and data acquisition software. The computer controls the entire system, writes the data to disk and performs the initial pedestal runs. The pedestal run takes 300 events in which it samples zero values (DC levels) of each channel, calculates the distribution of ADC values and makes an average which can be used to suppress unwanted sampling of events produced by electronic noise. The acquisition software also permits some initial analysis of the data in the form of two dimensional plotting of track events, time histograms and more. This allows the experimental set-up to be tuned before any data is recorded to disk. Without these tools as reference, the design of the analysis and track-finding software (see appendix section 6.3) would not have been possible.

3 Experimental set-up and methodology

The TPCp had been unused for several years and it had never been used with more than one FEC. The first task was to methodically test all of its individual components. This meant bringing the voltage across the GEMs and chamber up to operational levels, assembling and testing the readout electronics as well as setting up the computers and software for data acquisition.

This section is divided into four subsections which logically follow the progression of the project. It covers the initial preparations before starting the TPCp for the first time, analysis of taking initial measurements, analysis of the first tracks produced by cosmic muons, measuring and characterizing an americium-beryllium neutron source and performing the main measurements with the same source on the TPCp. Information on the design and implementation of the track reconstruction and analysis software which was developed as part of this project can be found in appendix section 6.3.

In addition to documenting the work which was done, this section will also act as a reference for future work regarding the TPCp.

3.1 Preparations and initial run

Firstly, the high voltage to the GEMs was carefully increased in small steps, since the system had not been used for several years, there was a concern that if the potential across the GEMs was increased too rapidly, they would spark and potentially get damaged. The same procedure was performed for the drift voltage supply across the TPC. For reference, the high voltage settings used during operations are included in Table 2.

Table 2: High voltage settings used during operations for the GEMs, main drift chamber and GEM shield.

Component	Supply [V]
Main drift chamber	-6000
GEM 3 Cathode	-450
GEM 3 Anode	-790
GEM 2 Cathode	-1190
GEM 2 Anode	-1530
GEM 1 Cathode	-1930
GEM 1 Anode	-2270
GEM shield	-2270

With these settings each GEM has an effective potential difference of 340 V between its anode and cathode. The supplied voltages are decreased from GEM 1 to GEM 3, where GEM 3 is closest to the padplane and the padplane itself is at ground potential (see Figure 10). From the settings in Table 2 the potential difference between the GEMs becomes 400 V, which is, taking into account the distance between them, low enough to not create any sparks an no avalanche amplification.

In order for the data acquisition software, getting data from the readout electronics, to know which part of the padplane corresponds to which channel on the FECs, each pad had to be allocated a coordinate which is then mapped to a unique channel. The TPCp has a padplane of 2016 individual pads, so a total of 16 FECs (16x128 channels) are needed to cover the entire padplane. This will leave 32 unused channels. Figure 14 shows a photo (a) of the padplane along with a schematic view (b). The alternating colors each correspond to a group of 16 channels which connect to one of the PCA16 and ALTRO chips on a FEC (see section 2.1 for more information). By relating the pads to a Cartesian coordinate system, data from each channel can be plotted to give a projected track image.

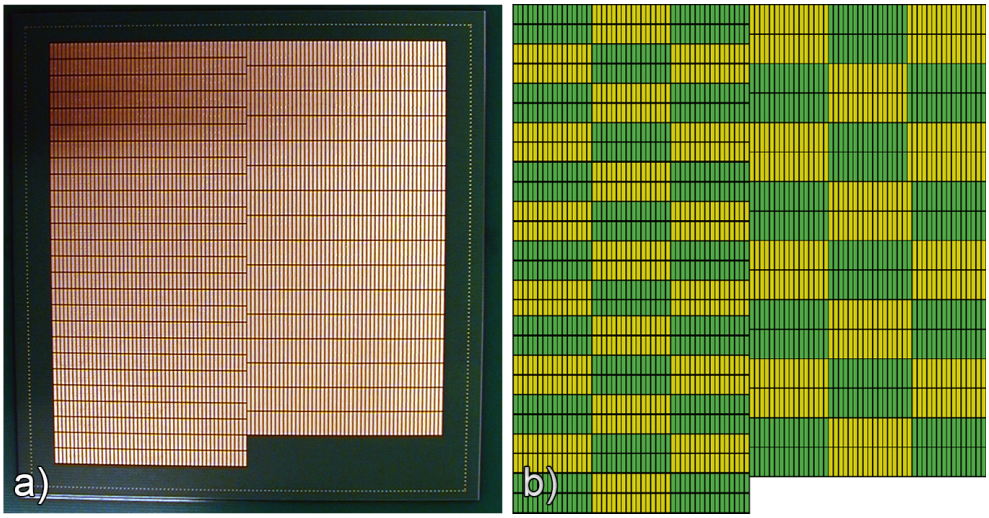

Figure 14: The left part of the figure shows the internally facing part of the TPCp's padplane, while the right part schematically shows the mapping and subsequent connector placement. The coordinate of each pad is individually mapped to a channel on one of the 16 FECs. The pads on the padplane have two areas each with two different pad sizes, 0.8x3.8 mm^2 and 0.8x5.8 mm^2. The spacing between pads is 0.2 mm [2].

The TPCp was flushed with an argon-carbon dioxide (Ar-CO_2) mixture (80% Ar and 20% CO_2), but while performing trial runs with the system it was quickly realized that the gas is needed to flush the chamber for about 48 hours (at 5 litres per hour) before any ionization events could be properly detected. It is reasonable to believe that this is caused by atmospheric air still remaining in the chamber, which absorbs most of the drifting electrons (see section 1.3.3). Once the chamber was operational, the flow of gas was left connected to the system until all measurements where done.

Lastly, table 3 contains the various RCU and trigger settings used during all measurement with the TPCp (see section 2.1 for more information). After some trial and error it was discovered that the pedestal runs would not execute properly at the normal trigger

frequency (152.6 Hz) used during measurements. The system could not write non-zero suppressed data fast enough to keep up with this trigger rate. So while doing the pedestal runs at the start of each measurement, the trigger rate was lowered to 38.15 Hz and then brought back up again to 152.6 Hz for the measurements.

Table 3: A list of settings for the RCU and the trigger frequencies used. The sample frequency of the ADC, number of samples recorded with each trigger, the frequency of the trigger (cosmic radiation excluded, see section 3.2) and number of events recorded are shown.

Measurements	Sample freq.	N. samples	Trigger freq.	Recorded events
Pedestal runs	20 MHz	-	38.15 Hz	300 events
Cosmic radiation	20 MHz	500	-	≈130 events
All other measurements	10 MHz	999	152.6 Hz	>200 000 events

3.2 First tracks

To create a controlled environment in which the source of the ionizing particle was known, cosmic radiation and a gamma source (cobalt-60) was used. Before measurements using a neutron source could be taken, an analysis of tracks produced by gamma radiation and cosmic radiation will lay the foundation needed to understand and interpret results using neutrons. This is because gamma interaction with matter (see section 1.2) and the ionizing effects of cosmic muons are both well known effects.

For the cosmic muons, the readout was triggered using two scintillators, one placed above and one below the TPCp. As a charged particle produces a signal in both scintillators above a certain threshold and within a time window of 50 ns, the RCU is triggered and records the event. Excluding any false triggers, where uncorrelated signals occur in both scintillators within the time window, the computer logs a significant amount of ionization events which show the characteristic straight tracks associated with high energy cosmic muons. Figure 15 shows an event from this dataset, where the upper part of the figure shows a three dimensional view and the lower part a two dimensional view of the same event. The range of ADC values and the average ADC value are both proportional to the ionization produced by the particle. So more ionization, or higher dE/dx, gives a higher ADC value.

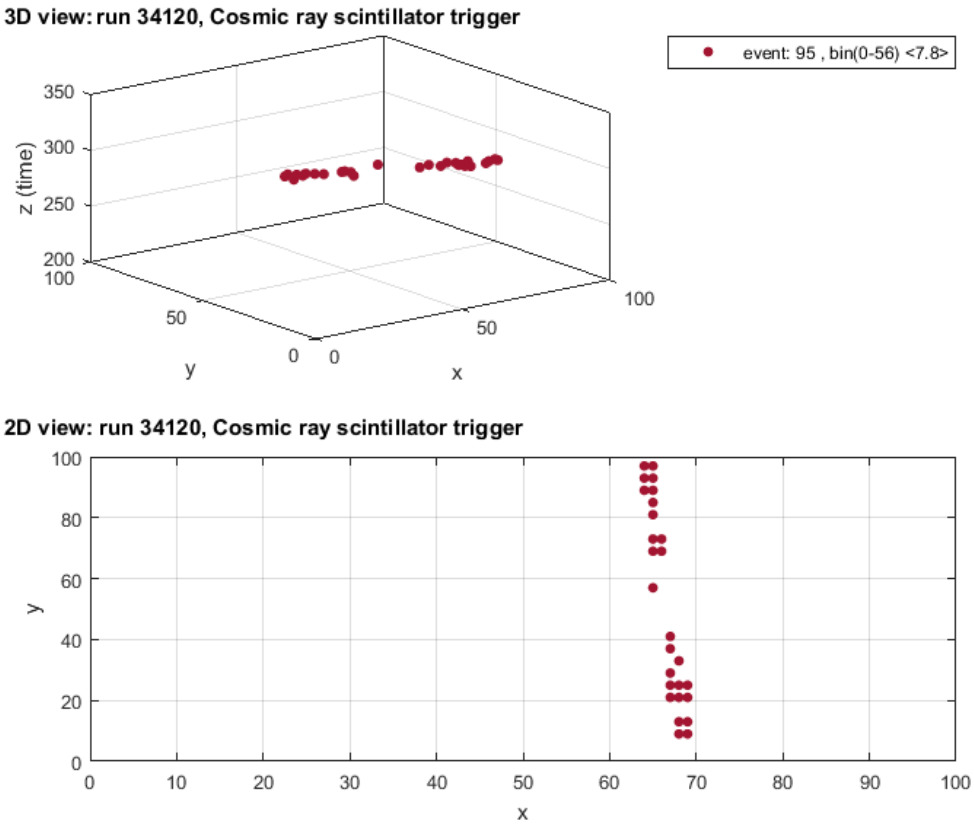

Figure 15: A three dimensional and two dimensional representation of an ionization track made by a cosmic muon. The legend shows the event number, range of ADC values and the average ADC.

As mentioned, the main goal is to understand how neutrons interact with the TPCp and one of the expected ways in which a thermal neutron would interact is through absorption into a nucleus. This would excite the nucleus and it would produce a gamma through de-excitation. Also, the source which was used (americium-beryllium) produced gamma radiation on its own. It is therefore an advisable next step to see how gamma radiation would interact with the TPC. A cobalt-60 source, which has the primary decay channel as seen in Eq. 5 below, was used.

$$^{60}_{27}\mathrm{Co} \rightarrow ^{60}_{28}\mathrm{Ni} + e^- + \bar{\nu}_e \tag{5}$$

Eq. 5 is a beta decay with a Q-value of 2.82 MeV. Two gamma rays are emitted from the excited ^{60}Ni nucleus with energies at 1.33 MeV and 1.17 MeV, respectively. Not many of the beta-electrons are expected to make it through the walls of the TPCp (0.8 mm material thickness, see figure 8) due to their relatively low energy (≈300keV). The TPCp should then primarily be radiated with gamma rays. Figure 16 is taken from the ^{60}Co measurement with the TPCp and shows an event which produced an irregular ionization pattern. The track is likely from a electron which originates from a gamma interaction with matter, like Compton scattering or pair production. From the figure it is clear that the point of origin lies outside the detectable area of the drift chamber, so most likely this electron comes from the chamber wall material of the detector.

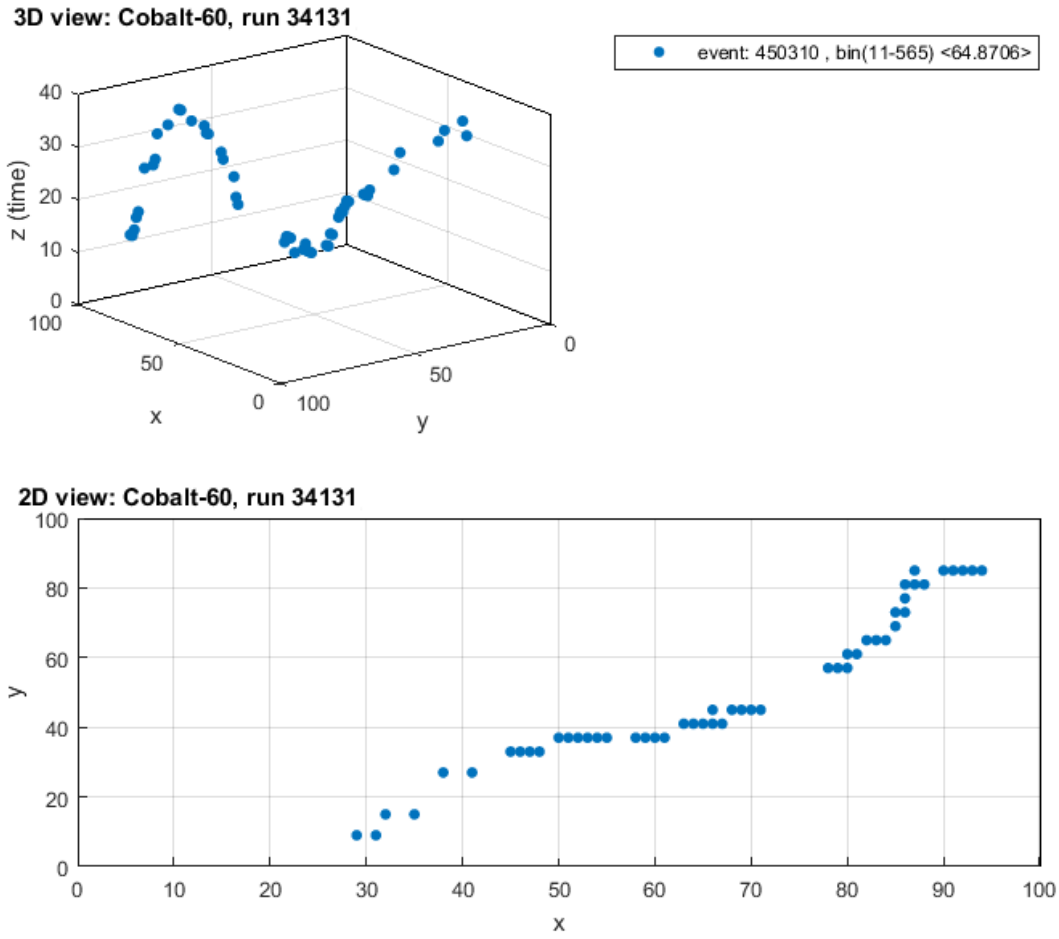

Figure 16: A three dimensional and two dimensional view of an ionization track, most likely from a Compton scattered electron due to gamma radiation. The legend shows the event number, range of ADC values and the average ADC.

What is interesting to note between figures 15 and 16 is that the average ADC values are different. The average ADC values are about 7.8 and 64.9 ADC units for the cosmic muon and ^{60}Co event respectively. Towards the end of its range the electron has a lower velocity than the cosmic muon, so, relating back to the theory of ionization (Eq. 3), this result further increases the confidence in the predicted cause of these tracks. Another difference is that the cosmic muon produces a straight track, while the electron scatters and changes direction along its path.

By assuming that the muon ionizes like a MIP, with an average energy loss of 2.44 keV/cm through argon [20], and measuring its track length, the dE/dx scale of the entire system can be roughly calibrated, converting ADC values to energy. Despite variations in the gas mixture and differences in pressure, the calibration is expected to be approximately valid for the forthcoming measurements since all other conditions were kept constant.

3.3 Characterization of the AmBe source

Before measuring with neutrons on the TPCp, from the AmBe source, several measurements were taken in an attempt to better understand at what rate neutrons and gammas radiate from the source. A YAP:Ce (Yttrium aluminium perovskite activated by Cerium) and a helium-3 (^{3}He) detector were used for the gammas and thermal neutron detection,

respectively. The source is made up of a mixture of ^{241}Am and ^{9}Be and has a total activity of 18.5 GBq. It produces a rate of 1.11 $\cdot 10^6$ neutrons per second isotropically in 4π steradians. Most of the activity thus comes from gamma emissions. These values will not be used directly but rather as a reference when measuring the expected rate at the TPCp from the source. The mechanism which produces free neutrons from the AmBe source (see Eq. 6 and 7) comes from the decay of ^{241}Am to an alpha-particle (α) and ^{237}Np. The ^{9}Be absorbs the α-particle, creating a free neutron and a 4.44 MeV gamma (γ) from the first excited state of ^{12}C. This is one of the most probable outcomes when ^{12}C is created from this decay chain but also includes the ^{12}C in its ground state or second excited state [14].

$$^{241}\mathrm{Am} \rightarrow {}^{237}\mathrm{Np} + \alpha \tag{6}$$

$$\alpha + {}^{9}\mathrm{Be} \rightarrow {}^{12}\mathrm{C} + n + \gamma\ (4.44\ \mathrm{MeV}) \tag{7}$$

In order to study the effects of the environment, a polyethylene moderator material, lead and borated plastic, was used between the source and the detectors in different configurations. The same configurations are then used while measuring with the TPC (section 3.4). Lead will help and block out the gamma rays produced by the source and the borated plastic has a specifically high cross-section for absorption of thermal neutrons. Although this absorption would produce more gamma rays from the subsequent excited boron in the plastic, the idea is to see a decrease in the amount of thermal neutrons which could be of value when discriminating between gammas and thermal neutrons in the analysis. The moderator material is made from high-density polyethylene (HDPE) and is enclosed in an aluminium container with a slot drilled out in the middle for the source. The higher energy neutrons (4–8 MeV) [9] produced from the source will "slow down" as they scatter while travelling through the polyethylene moderator, in effect loosing energy and becoming "thermal".

The ^{3}He detector is, as the name suggests, a helium-3 filled gas detector which absorbs the incoming neutrons and, through a nuclear reaction with a ^{3}He nucleus (Eq. 8) creates secondary charged particles that ionize the gas in the detector. This reaction has a very high cross section, giving the ^{3}He detector a very high efficiency for neutrons. Through this ionization the particles deposit their energy in the detector and create a pulse which indicates one neutron detected. The ^{3}He detector detects these nuclear products at a single central anode wire, which has a potential in the range of 1000-2000 V and is stretched across the length of the the detector. Such detectors are also sometimes referred to as a "single wire proportional counter".

$$n + {}^{3}\mathrm{He} \rightarrow {}^{3}\mathrm{H} + p + 0.764\ \mathrm{MeV} \tag{8}$$

The YAP:Ce detector is an inorganic scintillator detector for gamma rays. The incident gamma rays excite the scintillator material (perovskite) [6] which, through de-excitation, creates secondary photons that are converted to electrons in a photocathode. The electrons are then multiplied in a PMT (Photomultiplier Tube) that creates a signal where the number of incoming photons is proportional to the deposited energy.

The ^{3}He and YAP:Ce detectors have a detection efficiency of 95% and 50% for thermal neutrons and gammas respectively. These numbers are approximate, since the energy of the incoming radiation needs to be taken into account, but still act as a reference point of what to expect when radiating the TPCp.

As shown in section 3.2, gamma radiation may be detected in the TPCp, so in an attempt to minimize the amount of gammas reaching the detector, a shield of 5 cm thick lead was used. For all measurements both detectors where placed at the same distance from the source and each configuration was measured with both the YAP:Ce and the ^{3}He detectors. For purposes of solid angle normalization, the AmBe source is assumed to radiate isotropically.

The following configurations were used during these characterization measurements:

- Background measurement (source in a shielded container, still in the same room).
- Unmoderated source only (Figure 17a).
- Unmoderated source and lead (5 cm).
- Unmoderated source and borated plastic (5 cm thick).
- Unmoderated source, lead (5 cm) and borated plastic (5 cm) (Figure 17d).
- Moderated source only.
- Moderated source and lead (5 cm) (Figure 17c).
- Moderated source and borated plastic (5 cm) (Figure 17b).

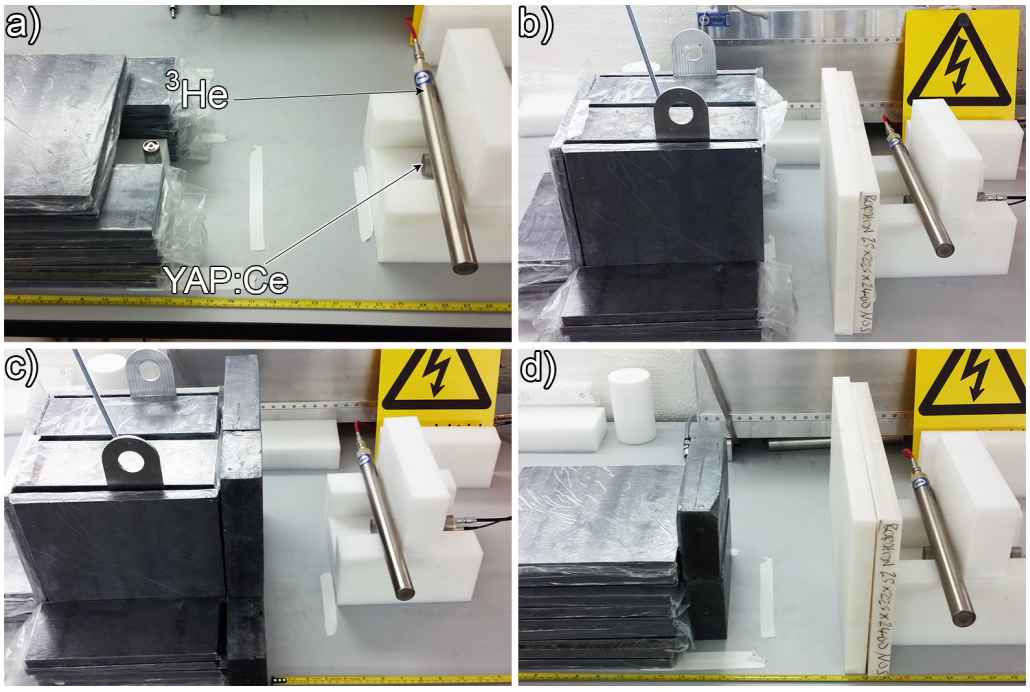

Figure 17: Using the YAP:Ce (small cylinder) and ^{3}He detectors (long cylinder), Figure a) shows measurement with the unmoderated source. Figure b) shows measurement with the moderated source and borated plastic (5 cm thick) as shielding. Figure c) shows measurement with the moderated source with lead (5 cm thick) as shielding. Figure d) shows measurement with the unmoderated source with lead (5 cm thick) and borated plastic (5 cm thick) as shielding. The moderator block for the source is encapsulated in a lead shield in an attempt to control the direction of the radiation. Photographs by author.

The results of these measurements are presented in table 4 below.

Table 4: Tabulated data of the measured rates per second from thermal neutrons and gamma rays for the YAP:Ce and ^{3}He detectors. All measurements are taken at 36 cm from the AmBe source and are normalized for time. The YAP:Ce detector is mostly sensitive to gamma. The rates from the ^{3}He detector is for thermal neutrons only, since they produce a certain energy deposit which decides the interval of integration.

Configuration	Detected particle type	Detector	Rate [s^{-1}]
Unmoderated	gammas	YAP:Ce	$1.41 \cdot 10^5$
Unmoderated+lead	gammas	YAP:Ce	$2.56 \cdot 10^2$
Moderated	gammas	YAP:Ce	$6.34 \cdot 10^2$
Moderated+lead	gammas	YAP:Ce	$6.05 \cdot 10^1$
Unmoderated	thermal neutrons	^{3}He	$9.49 \cdot 10^2$
Unmoderated+lead	thermal neutrons	^{3}He	$9.13 \cdot 10^2$
Unmoderated+lead+boron	thermal neutrons	^{3}He	$5.76 \cdot 10^2$
Moderated	thermal neutrons	^{3}He	$1.69 \cdot 10^3$
Moderated+lead	thermal neutrons	^{3}He	$1.33 \cdot 10^3$
Moderated+boron	thermal neutrons	^{3}He	$3.19 \cdot 10^2$

Figures 18 and 19 show the results for four of the different experimental set-ups regarding gammas (YAP:Ce detector) and thermal neutrons (^{3}He detector), respectively. For figure 18, the full absorption peak of the 4.44 MeV gamma from the first excited state of ^{12}C is noted in the spectrum. This "plateau" contains the first and second escape peaks, where only part of the gammas energy was deposited in the detector.

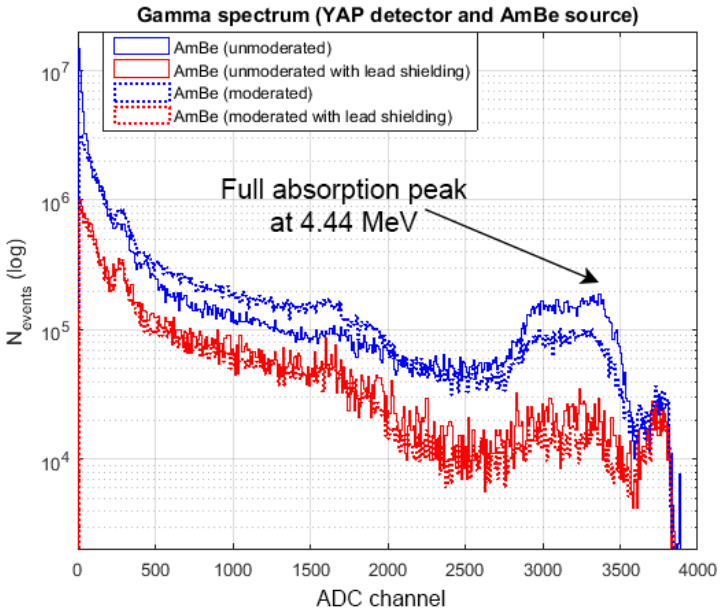

Figure 18: Gamma measurements taken using a YAP:Ce detector with an AmBe source. Unshielded source is blue and lead shielded source is red. The solid lines represent the unmoderated source while, dotted lines represent the moderated source.

Figure 19 shows the spectrum measured with the ^{3}He detector and notes the different "peaks" resulting from complete and partial absorptions of the nuclear reaction products

(see Eq. 8). The first peak (191 keV) is where the proton hits the wall of the detector and only the triton is absorbed. The second peak (573 keV) is where the triton hits the wall of the detector and only the proton is absorbed. The last peak (764 keV) corresponds to the absorption of both the triton and proton in the detector gas [14]. The total rate is given by integrating over this entire area, since the detection of either a triton, proton or both correspond to one neutron being absorbed in the ^{3}He gas.

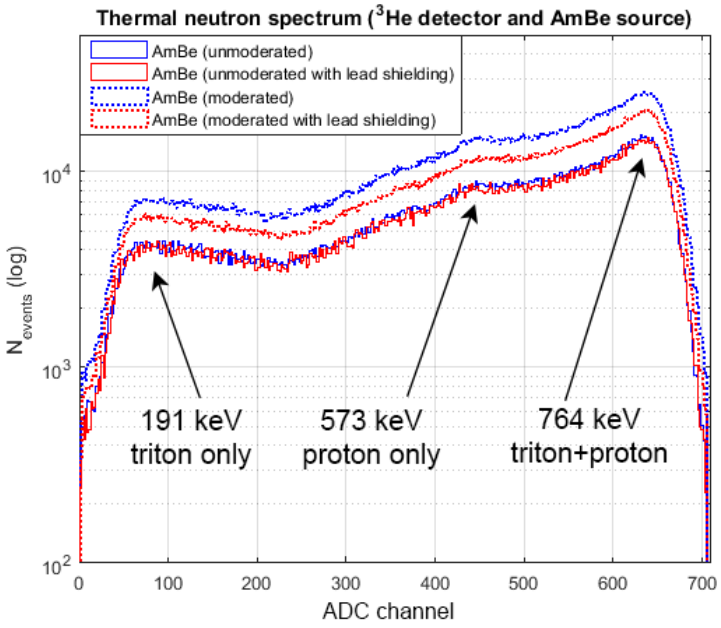

Figure 19: Thermal neutron measurements taken using a ^{3}He detector with an AmBe source. Unshielded source is blue and lead shielded source is red. The solid lines represent the unmoderated source, while dotted lines represent the moderated source. The full spectrum is shown in appendix section 6.2, figure 24.

3.4 Measurement with the TPCp

The final measurements were taken with the AmBe source at the TPCp using the same experimental configurations as explained in section 3.3. The AmBe source remained at a fixed distance (39.9 cm) from the center of the TPCp for all measurements. Figure 20 shows the experimental set-up while measuring using a moderated source, lead shield and borated plastic.

For each measurement the data was analysed by making histograms of the total energy deposited (figure 22) and running it through a track-finding program. The track-finding program is discussed in appendix section 6.3.

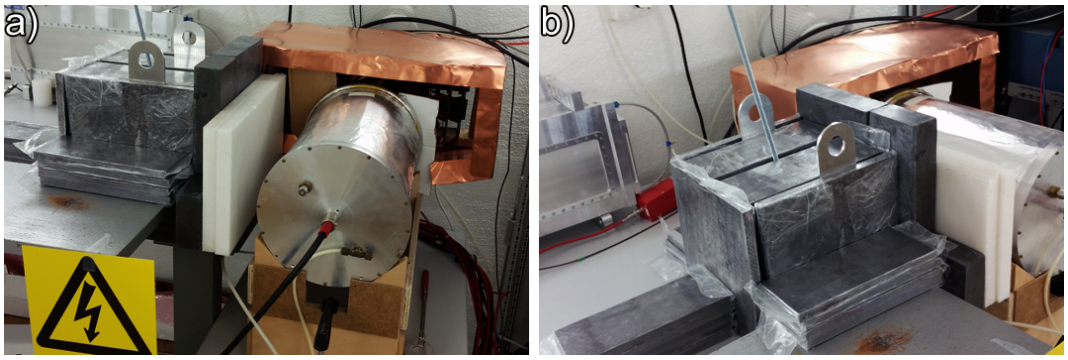

Figure 20: Figure a) and b) show the experimental set-up while measuring with a moderated AmBe source using lead shielding (5 cm thick) and borated plastic (5 cm thick) in front of the TPC. The source is encapsulated in a lead shield in an attempt control the direction of the radiation. Photographs by author.

4 Analysis of TPCp measurements and results

The first step in the analysis was to inspect tracks in order to see if track produced by gammas, fast neutrons and thermal neutrons could be distinguished. Data with an unshielded and unmoderated source should contain mostly fast neutrons and gammas. Here one can clearly recognize short tracks with a large amount of energy deposited. Figure 21 is a typical example of such track. Relating to figure 22 for this configuration it is clear that there is an enhanced number of events at these higher energy deposits. For other configurations there is no obvious difference, neither concerning tracks nor concerning deposited energy.

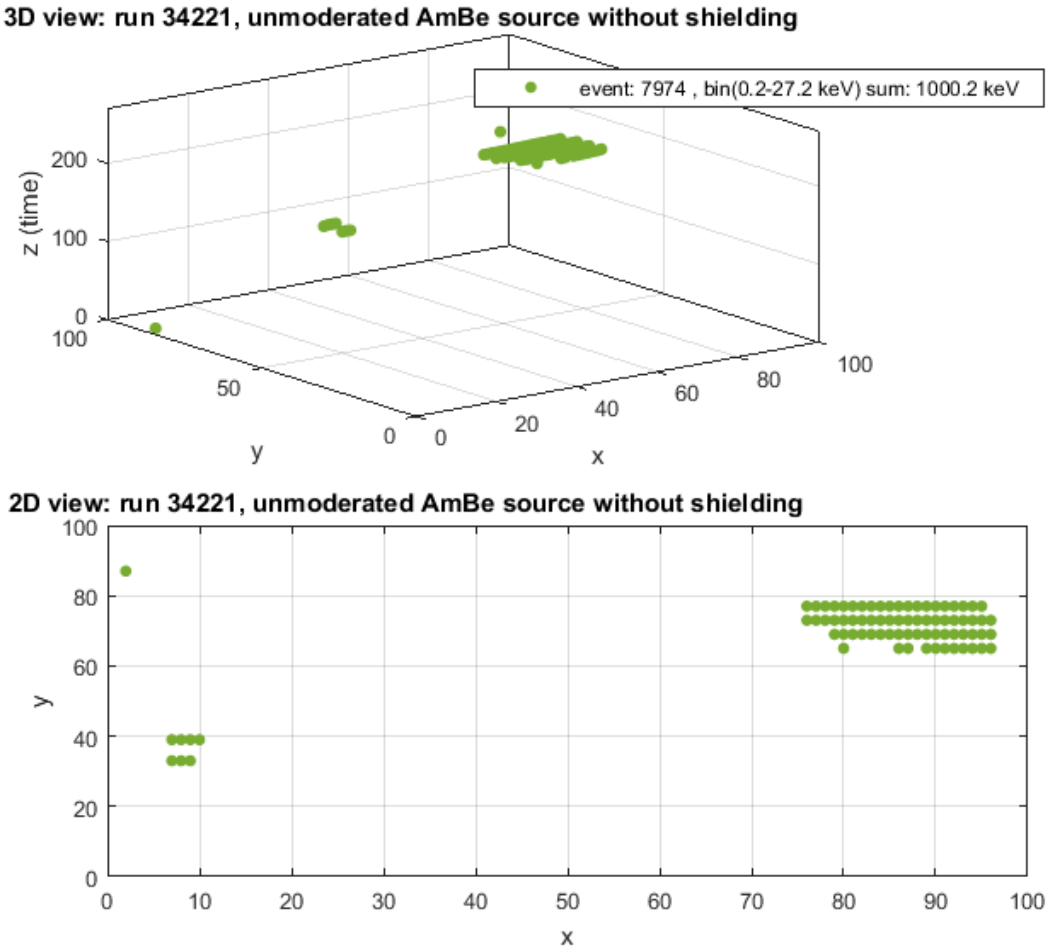

Figure 21: A three dimensional and two dimensional view of an ionization track, most likely from a fast neutron interaction with the TPC. The legend shows the event number, range of energy, average energy and the total energy deposited.

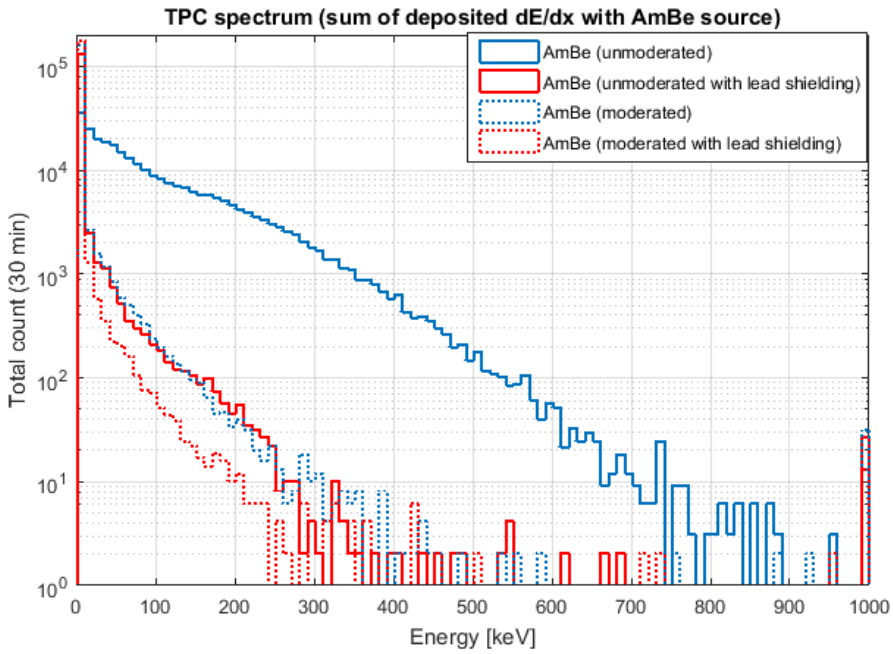

Figure 22: Sum of deposited energy for each event using the TPCp with an AmBe source. Unshielded source is blue and lead shielded source is red. The solid lines represent an unmoderated source, while dotted lines represent a moderated source.

The approach was then to extract the thermal neutron detection rate by subtracting the estimated number of events caused by gamma interaction from the total number of events and thus obtain the estimated events which correspond to interactions by thermal neutrons. First, the TPCp's efficiency for gamma detection needed to be determined. This was achieved by analysing measurements taken with the AmBe source unmoderated and unshielded, where the rate of thermal neutrons is about 0.02% of the rate of gammas. These few neutrons are assumed to be negligible for this efficiency estimate. By then dividing with the expected exposure rates, given by the YAP:Ce detector measurements, the gamma detection efficiency for the TPCp could be obtained. The detection rate of gammas could then be calculated and subtracted for each measurement. Using the expected exposure rates measured by the ^{3}He detector then gives the detection efficiency of thermal neutrons for the TPCp. This efficiency is only available for the two configurations which use a moderated AmBe source, since the expected exposure rates measured with the ^{3}He detector only apply to thermal neutrons. In all cases the expected exposure rate at the TPC was calculated by normalizing the YAP:Ce and ^{3}He measurements with regards to their solid angle and efficiencies. Table 5 shows the results discussed here.

Reference guide to the different variables used for the calculations in table 5.
$\mathbf{A^{\gamma}_{TPC}}$, $\mathbf{A^{n}_{TPC}}$: expected exposure rates per second of γ or n at TPCp (based on measurements with the YAP:Ce and ^{3}He detectors).
$\mathbf{N^{tot}_{TPC}}$: the measured total rates per second from TPC.
$\mathbf{N^{\gamma}_{TPC}}$, $\mathbf{N^{n}_{TPC}}$: calculated rates from TPC of γ and n.
η_{γ}, $\eta_{\mathbf{n}}$: calculated detection efficiency of γ and n for TPC.

Table 5: Table of data from the measured and calculated rates and detection efficiencies of the TPCp. Associated to each column is a letter which is used to describe the calculations. A, B: expected exposure rates at the TPCp for gammas and thermal neutrons, C: the total measured rate of tracks by the TPCp (see appendix section 6.3 for explanation), D: calculated gamma rate detected at TPCp, E: calculated thermal neutron rate detected at the TPCp, F, G: detection efficiency of gammas and thermal neutrons for the TPCp. The rate enclosed in parenthesis is not calculated but rather approximated to contain a negligible amount of neutrons. (*)The value for the gamma efficiency is an upper estimate, assuming that all detected particles are gammas, which is obviously not quite the case. For step-by-step calculations of the rates in column A and B see appendix section 6.1. For calculations of the efficiencies in column F and G see appendix 6.2.

	A	B	C	D	E	F	G
				C-E	C-F·A	D/A	E/B
	A^{γ}_{TPC}	A^{n}_{TPC}	N^{tot}_{TPC}	N^{γ}_{TPC}	N^{n}_{TPC}	η_{γ}	η_{n}
Unmoderated	$1.22 \cdot 10^7$	$2.82 \cdot 10^3$	$5.25 \cdot 10^3$	$(5.25 \cdot 10^3)$		0.04%*	
Unmoderated+lead	$2.21 \cdot 10^4$	$2.71 \cdot 10^3$	$1.12 \cdot 10^2$	$9.57 \cdot 10^0$			
Moderated	$5.47 \cdot 10^4$	$5.02 \cdot 10^3$	$1.93 \cdot 10^2$	$2.37 \cdot 10^1$	$1.70 \cdot 10^2$		3.38%
Moderated+lead	$5.22 \cdot 10^3$	$3.96 \cdot 10^3$	$5.87 \cdot 10^1$	$2.26 \cdot 10^0$	$5.64 \cdot 10^1$		1.42%

Since the η_{γ} is an upper estimate of the gamma efficiency for the TCPp, the calculated neutron efficiency (η_n) will be a lower limit. This is primarily reflected in the difference resulting from moderated and moderated with lead shielding.

5 Outlook and reflections

Work performed as part of this report was an initial study, where it was of importance to go through all steps of the procedure. If it would be possible to reach a reliable value of the neutron detection efficiency, this could be considered a bonus. Unfortunately, there were no possibilities to go back, repeat and improve measurement based on analysis of the results within the time frame of this thesis. To improve understanding of the mechanisms and physical effects behind the measurements it is recommended to run a Geant-4 simulation before measurements in the future.

Based on the stopping power in argon (at 1 atm) for protons and electrons, their respective stopping range can be calculated (Table 6) and compared with reconstructions of tracks and deposited energy.

Table 6: Calculated expected stopping distances for a proton and electron in argon at 1 atm pressure. Calculations made with data from NIST [3].

Particle	Energy (keV)	Stopping distance (cm)
Electron	200	36.47
	500	343.30
	1000	450.04
Proton	200	0.29
	500	0.92
	1000	2.51

It is then evident that the track in figure 21 is not from an electron, since the track in relation to the deposited energy is too short. It does more coincide with the expected ionization from a proton, which could have originated from the nuclear reaction between a fast neutron (4-8 MeV) from the AmBe source and a nucleus. Even though the gas used in the TPCp is not pure argon but rather a Ar-CO_2 mixture, the calculations in table 6 are assumed to be a good approximation of what we expect to see.

Observations made during the experiments with the TPCp have given insight towards future improvements which can be made. A new layout for the padplane, which is less dependent of the ionizing particles direction, would improve the tracking. A hexagonal pad shape (see figure 23) would produce tracks of similar response and be less dependent on the direction of the particle. Compare figures 7 and 23.

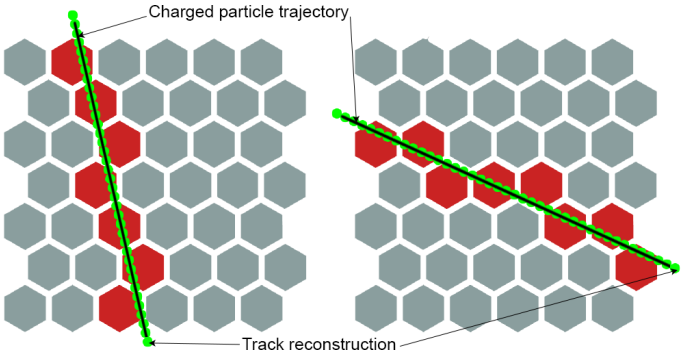

Figure 23: The proposed hexagonal pad shape. Red color indicates pads which have received signals over threshold from the ionization. Black line is the trajectory of the charged particle, and the dotted green line is the reconstructed path. Schematic view shows 42 channels.

Due to time constrains, the track-finder and plotting program which was designed and used for the analysis does not include a center-of-gravity calculation between the pads for a more accurate reconstruction of the track. Also, the software should be redesigned with the option of visualizing a color coded pulse height for each coordinate of the track, which would produce a more comprehensive view of the track. Lastly, the track-finding algorithm should be completely redesigned to be less resource intensive. With better track information it may be possible to distinguish between thermal neutron events and gamma events, which would reduce the importance of determining a correct gamma efficiency. Calculating the detection efficiency for thermal neutrons (η_n) was based on first approximating and calculating the efficiency for gammas (η_γ) (see appendix section 6.2). This detection efficiency for thermal neutrons could be more reliably determined with a gamma source which does not emit any neutrons. It would however be important to have spectrum of gammas which is comparable with the energies from the AmBe source (goes up to 4.44 MeV) Again, simulations would be a good way to start.

The high energy gammas (4.44 MeV) from the AmBe source are closely related to the emission of a neutron. The gammas originate from the first and second excited states of the ^{12}C nucleus after neutron emission. These gammas could conceivably act as trigger mechanism for the TPCp's readout electronics.

Occasionally, after running the pedestals there would be channels which are continuously sampled even though there had been no ionizing event in the chamber. After another pedestal run these channels would work properly again, or another might stop working. This gives rise to some unwanted differences between the measurements which could be solved by running all measurements with the same pedestal run. This could include slightly higher sampling values per ADC channel, which would slightly change the rates in figure 22. The best thing would have been to re-run all measurements after initial testing and set-up was finished. This was not done due to time limitations.

The rates ($N_{\mathrm{TPC}}^{\mathrm{tot}}$) in table 5, column C, is the number of events per second which has been selected to correspond to actual tracks. This is decided by the track-finding software which was designed for this project. For an overview of the selection process see appendix section 6.3. Limitation exists for the software in the case of events with more than one track or events which have a slightly higher noise. The program could potentially exclude these from the search. The development of a "smarter" and and more resource efficient track-finding program is recommended for future work with the TPCp.

The main goal of this thesis was to put together a test stand and procedure with which, using information presented in this report as reference, future experiments with the TPCp can be made. This has successfully been achieved and further results presented as part of this report is more to get a preliminary idea of how neutrons actually interact with a TPC. With this in mind, no error calculations have been made for the efficiency calculations of gammas and thermal neutrons. For these, uncertainties exist through the calculations of the solid angles, the rates at the TPCp calculated from the track-finding software and the efficiencies of the YAP:Ce and ^{3}He detectors at the specific energies produced from the AmBe source.

6 Appendix

6.1 Calculation of expected exposure rates for the TPCp

To calculate the expected rate of both gammas and thermal neutrons at the TPCp, the total counts were normalized to a live time of 500 seconds for each detector. In the case of the ^3He detector, only bins 146 to 850 were included. The lower bin limit corresponds to events where only energy from one of the two reaction products (Eq. 8) is deposited in the gas. Anything over bin 850 is also cut from the calculations, since it is above the "plateau" where the full energy of the nuclear reaction is captured. The integrated number of events in the 146-850 window is then expected to be thermal neutrons only.

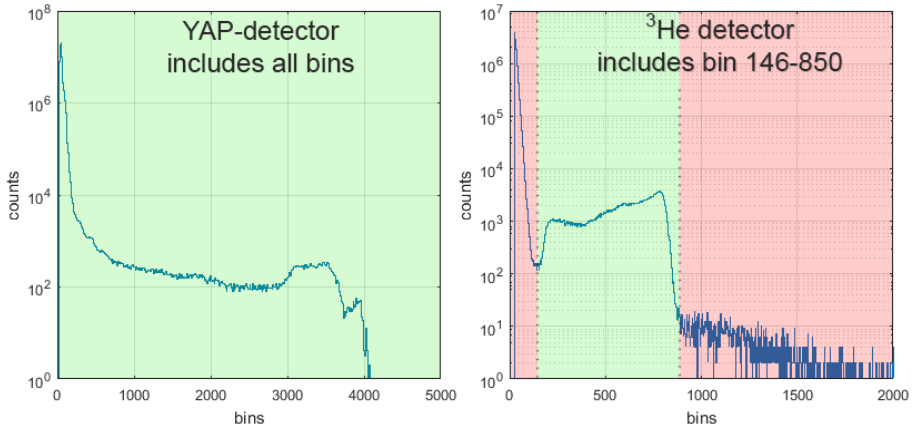

Figure 24: Examples of histograms for both the YAP:Ce and the ^{3}He detector. Green and red color indicates the intervals which are included and excluded from the rate calculations, respectively.

To get the expected rate of gammas ($A^{\gamma}_{\mathrm{TPC}}$) and thermal neutrons ($A^{n}_{\mathrm{TPC}}$) at the TPCp, first, the solid angles (Ω_{YAP}, Ω_{He}) of the two detectors and the solid angle of the TPCp (Ω_{TPC}) relative the the AmBe source are calculated. This is done by comparing their projected areas relative to the distance from the source r for the YAP:Ce and ^{3}He detectors and r' for the TPCp:

$$\Omega_{\mathrm{YAP}} = \frac{\mathrm{YAP}_{\mathrm{area}}}{4\pi r^2}$$

$$\Omega_{\mathrm{He}} = \frac{\mathrm{He}_{\mathrm{area}}}{4\pi r^2}$$

$$\Omega_{\mathrm{TPC}} = \frac{\mathrm{TPC}_{\mathrm{area}}}{4\pi r'^2}$$

The expected rate at the TPCp, $A^{\gamma}_{\mathrm{TPC}}$ and A^{n}_{TPC} is calculated from the rate measurements, N_{YAP} and N_{He}, performed with the YAP:Ce and ^{3}He detectors, respectively. These rates are normalized with respect to the TPCp's solid angle coverage compared with the coverage from the YAP:Ce and ^{3}He detectors. The efficiencies of the YAP:Ce (η_{γ}) and ^{3}He (η_n) detectors are also included:

$$A^{\gamma}_{\mathrm{TPC}} = N_{\mathrm{YAP}} \cdot \frac{\Omega_{\mathrm{TPC}}}{\eta_{\mathrm{YAP}} \cdot \Omega_{\mathrm{YAP}}}$$

$$A^{n}_{\mathrm{TPC}} = N_{\mathrm{He}} \cdot \frac{\Omega_{\mathrm{TPC}}}{\eta_{\mathrm{He}} \cdot \Omega_{\mathrm{He}}}$$

For each set-up the TPCp was placed at $r' = 39.9$ cm and the YAP:Ce and ^{3}He detectors at $r = 35.8$ cm from the source. These distances are to the center of the respective detectors. The areas for the respective detectors are $\text{YAP}_{\text{area}} = 4.9$ cm^2, $^3\text{He}_{\text{area}} = 75$ cm^2 and $\text{TPC}_{\text{area}} = 263$ cm^2. Efficiencies for the detectors are $\eta_{\text{YAP}} = 50\%$ and $\eta_{\text{He}} = 95\%$. Now, the expected rates A^{γ}_{TPC} and A^{n}_{TPC} can be calculated using the measurements presented in table 4.
Unmoderated source:

$$A^{\gamma}_{\text{TPC}} = 1.41 \cdot 10^5 s^{-1} \cdot \frac{0.0131}{0.5 \cdot 0.000305} \approx 1.22 \cdot 10^7 s^{-1}$$

$$A^{n}_{\text{TPC}} = 9.49 \cdot 10^2 s^{-1} \cdot \frac{0.0131}{0.95 \cdot 0.004605} \approx 2.82 \cdot 10^3 s^{-1}$$

Unmoderated source with lead shield:

$$A^{\gamma}_{\text{TPC}} = 2.56 \cdot 10^2 s^{-1} \cdot \frac{0.0131}{0.5 \cdot 0.000305} \approx 2.21 \cdot 10^4 s^{-1}$$

$$A^{n}_{\text{TPC}} = 9.13 \cdot 10^2 s^{-1} \cdot \frac{0.0131}{0.95 \cdot 0.004605} \approx 2.71 \cdot 10^3 s^{-1}$$

Moderated source:

$$A^{\gamma}_{\text{TPC}} = 6.34 \cdot 10^2 s^{-1} \cdot \frac{0.0131}{0.5 \cdot 0.000305} \approx 5.47 \cdot 10^4 s^{-1}$$

$$A^{n}_{\text{TPC}} = 1.69 \cdot 10^3 s^{-1} \cdot \frac{0.0131}{0.95 \cdot 0.004605} \approx 5.02 \cdot 10^3 s^{-1}$$

Moderated source with lead shield:

$$A^{\gamma}_{\text{TPC}} = 6.05 \cdot 10^1 s^{-1} \cdot \frac{0.0131}{0.5 \cdot 0.000305} \approx 5.22 \cdot 10^3 s^{-1}$$

$$A^{n}_{\text{TPC}} = 1.33 \cdot 10^3 s^{-1} \cdot \frac{0.0131}{0.95 \cdot 0.004605} \approx 3.96 \cdot 10^3 s^{-1}$$

These values are presented in the results section, table 5.

The solid angle estimates are difficult due to the cylindrical shapes of the detectors, the fact that the TPCp has a larger gas volume than the instrumental volume, as well as the probability that a gamma may convert in the walls of the TPCp and the electron enters the instrumented volume.

6.2 Calculation of actual rates for the TPCp

Relating the calculated expected rates at the TPCp with an unmoderated AmBe source between the YAP:Ce ($A^{\gamma}_{\mathrm{TPC}}$) and ^{3}He detector ($A^{n}_{\mathrm{TPC}}$) (see table 5 column A and B), the rate of thermal neutrons is about 0.02% the rates of gammas, so as an approximation the thermal neutron rate were ignored and an efficiency for the detection of gammas (η_γ) can be calculated.

$$\eta_\gamma = \frac{N^{\gamma}_{\mathrm{TPC}}}{A^{\gamma}_{\mathrm{TPC}}} \Rightarrow \frac{5.25 \cdot 10^3 s^{-1}}{1.21 \cdot 10^7 s^{-1}} \approx 0.0004$$

Were $N^{\gamma}_{\mathrm{TPC}}$ is the rate measured by the TPC and $A^{\gamma}_{\mathrm{TPC}}$ is the expected gamma exposure, measured with the YAP:Ce detector.

Applying η_γ to the rates in table 5 the relative amounts of gammas can be removed and the remaining rate is that of the thermal neutrons (N^{n}_{TPC}).

$$N^{n}_{\mathrm{TPC}} = N^{\mathrm{tot}}_{\mathrm{TPC}} - \eta_\gamma \cdot A^{\gamma}_{\mathrm{TPC}} \Rightarrow$$

$$N^{n}_{\mathrm{TPC}} = 1.93 \cdot 10^2 s^{-1} - 0.0004 \cdot 5.47 \cdot 10^4 s^{-1} \approx 1.70 \cdot 10^2 s^{-1}$$

and

$$N^{n}_{\mathrm{TPC}} = 5.87 \cdot 10^1 s^{-1} - 0.0004 \cdot 5.22 \cdot 10^3 s^{-1} \approx 5.64 \cdot 10^1 s^{-1}$$

The efficiency for detecting thermal neutrons at the TPC (η_n) can then be calculated in the same way as for gammas using the expected rates in table 5.

$$\eta_n = \frac{N^{n}_{\mathrm{TPC}}}{A^{n}_{\mathrm{TPC}}} \Rightarrow$$

$$\eta_n = \frac{1.70 \cdot 10^2 s^{-1}}{5.02 \cdot 10^3 s^{-1}} \approx 3.38\%$$

and

$$\eta_n = \frac{5.64 \cdot 10^1 s^{-1}}{3.96 \cdot 10^3 s^{-1}} \approx 1.42\%$$

6.3 Track-finding and histogram programs

It is roughly estimated that around 40% of the time spent on this project was devoted to designing and coding the track-finding and histogram plotting software. This includes the initial mapping of coordinates and addresses to allow for the TPCs readout electronics to distinguish between the different pads on the padplane. All software used for this project was designed and written in MATLAB®[1]. Since MATLAB is taught within the Physics Bachelor programme, this was used in spite of a possible better efficiency if C++ had been used.

Track-finding program

Each measurement taken at the TPC is saved in text files which than can be imported into the track-finding program. Each text file corresponds to an experimental set up, described in section 3.3. Each file will contain about 200'000 events.

- Formatting:

The imported data gets formatted in three steps: Each event number is removed and stored in a separate variable, the ADC sampling for each pad is replaced with its maximum value and each pad gets assigned its corresponding x and y coordinates.

- ADC filter:

A pre filter will then compare the maximum ADC sample from each pad with a threshold parameter and remove any pad from the data set which is less. This is to make the program run faster in the case only higher ADC values are needed for the run. Can be put to zero which would let every single pad through.

- Drift time:

With the time stamp from the readout electronics, the z-coordinate can be calculated. It uses the average drift velocity of the TPCp (0.75cm/μs at 6000 V).

- Plot index:

A separate variable containing all the coordinates of all the fired pads in an event is created. This is is the most resource intensive part of the program. This "plot index" is needed so that each event can easily be plotted as a separate entry. Also, as part of this step, an index for the event number is created in an identical manner. This index is later used as a reference, so that further logic is applied on an event-to-event basis.

- Track-finding:

Firstly, the plot index is sorted from closest to origo to furthest away. Using a set number of parameters, the program scans through the plot index looking for the distance between each coordinate entry. These distances are compared against a pre-set variable r. If the distance is greater than r, the event gets flagged with a "fail-point", and if it is the same or less than r it gets flagged with a "pass-point". After, the program goes to the next coordinate in the event. The "points" are accumulative, and if enough "fail-points" are allocated the event gets rejected and the program goes to the next event. If enough "pass-points" are allocated, the event gets kept and the program goes to the next event. The minimum distance (r) between the coordinates, limit for "pass-points" and "fail-points" are all modifiable variables.

For all data collected in this report the settings were: distance 2 mm, fail-points: 2, pass points: 10. This also means that an event needs to have atleast 10 pad entries to be able to pass as a track.

[1] version 8.6.0.267246 (R2015b)

This way of looking for tracks is not the most ideal, since if there were to be coordinates close to origo which originate from background noise, or other unfavourable sources, these would still be counted. Also, and most importantly, it does not take into account events with more than one track.

- Legend and Plotting:

The minimum and maximum ADC value, average ADC value and event number are then collected and put into a plot legend. This part also has the option of calculating and including the root means square and/or standard deviation for each event. All ADC values can be converted to energy using the calibration done in section 3.2 (29 eV/ADC). All events are then plotted and the plot legend is included. A two dimensional view and three dimensional view are both displayed (see for example figures 15 and 16).

- Rate calculation:

Based on the number of events (N) which the track-finding algorithm passed as tracks, the program displays the calculated rate (R) of the data set, Eq. 9.

$$R = \frac{N \cdot T}{i_{max} \cdot \delta} \tag{9}$$

Where T is the trigger rate in Hz ($T = 152.6$ Hz) and i_{max} is the maximum event number in in the data set. Since each trigger will record one event, the event number i is directly related to the measured time. δ is the time coverage (δ =1.53%). The time coverage is there to normalize the rate to events per second. Events per second is the standard with which all calculations are performed in this report.

Histogram plotting

This program takes the same data file as the track-finding program as input.

- Formatting:

Exactly the same formatting as for the track-finding program is used here as well, but no information about the x and y coordinates is stored.

- Calculating average and sum:

Going through the ADC values belonging to each event, the average ADC value (for non zero pads) as well as the sum of all ADC values, are calculated on an event-to-event basis. At this point no information about the event id is kept, and the resulting variables are simply lists of all the calculated sum and average ADC values, respectively.

- Normalizing:

Using information supplied in the original data file about the recording time, both variables can be normalized with respect to time.

- Plotting:

Using customizable built in functions like `histogram()`, the average and sum data sets are individually plotted.

The software is able to go through these steps for either the average or the sum of ADC values, and has a third option to import and subtract a background measurement.

Acknowledgements

I would especially like to thank my supervisor *Professor Anders Oskarsson* for giving me the opportunity to work with such an interesting project. His patience with me and expertise in the subject matter made the entire process very enjoyable.

A huge thanks to *Dr Ulf Mjörnmark* who took extra time to answer my questions, provide comments to my initial draft of this report and taught me about the data acquisition software and electronic readout systems. I also got some insight into programming which I am sure will benefit me greatly in future work.

I further would like to thank *Professor Leif Jönsson* for supplying useful reading material regarding the TPCp and sharing his experience.

I would also like to thank *Herjuno Nindhito*, *Patrawan Pasuwan* and *Rickard Lydahl* for providing a pleasant working environment and for discussing subject matters related and unrelated to physics with me.

Finally, the experimental work using the AmBe source was made possible thanks to the Detector Group of the European Spallation Source and the Source-based Neutron Irradiation Group of the Division of Nuclear Physics (SoNnIG) at Lund University who supplied the radioactive materials, detectors for characterizing the source and made available their facilities to perform our work. A special thanks to *Associate Professor Kevin Fissum*, *Dr Hanno Perrey*, *Julius Scherzinger*, *Dr Mikael Elfman* and *Professor Per Kristiansson* who all made time for me and my questions regarding nuclear physics and beyond. Thank you.

All in all, this project has simultaneously been the most stressful and greatest learning experience during my time at the university. Above all else, in no small part thanks to the aforementioned people, I had a great time!

References

[1] ESS Cnseptual Design Report. http://esss.se/documents/CDR_final_120206.pdf. Accessed: 2016-01-19.

[2] EUDET Detector R&D Lund University. http://www.hep.lu.se/eudet/. Accessed: 2015-12-10.

[3] NIST National Institute of Standards and Technology: Physical Measurement Laboratory. http://http://www.nist.gov/pml/data/star/. Accessed: 2015-12-16.

[4] The Altro chip user manual. http://ep-ed-alice-tpc.web.cern.ch/ep-ed-alice-tpc/doc/ALTRO_CHIP/UserManual_draft_02.pdf. Accessed: 2016-01-19.

[5] Abe, K., Hayato, Y., Iida, T., Ishihara, K., Kameda, J., Koshio, Y., Minamino, A., Mitsuda, C., Miura, M., Moriyama, S., et al. (2015). Search for n- n^- oscillation in Super-Kamiokande. *Physical Review D*, 91(7):072006.

[6] Baccaro, S., Blaŝek, K., De Notaristefani, F., Maly, P., Mares, J., Pani, R., Pellegrini, R., and Soluri, A. (1995). Scintillation properties of yap: Ce. *Nuclear Instruments and Methods in Physics Research Section A: Accelerators, Spectrometers, Detectors and Associated Equipment*, 361(1):209–215.

[7] Behnke, T., Hallermann, L., Schade, P., and Diener, R. (2006). The field cage for the Large TPC Prototype. *EUDET-Memo-2006-03, EUDET*.

[8] Brooijmans, G. and et al. (2015). Expression of Interest for A New Search for Neutron-Anti-Neutron Oscillations at ESS. *2014/2015 Round, Instrument Construction Proposal*.

[9] Browne, E. (2000). Commonly used radioactive sources. *The European Physical Journal C-Particles and Fields*, 15(1):190–194.

[10] Ferbel, T. (1987). *Experimental techniques in high-energy nuclear and particle physics*. World Scientific.

[11] Group, P. D. et al. (2008). Experimental methods and colliders. *Physics Letters B*, 667(1):261–315.

[12] Hedberg, V., Jönsson, L., Lundberg, B., Mjörnmark, U., Oskarsson, A., and Osterman, L. (2012). Development of the Readout System for a TPC at the Future Linear Collider. *LC-DET-2012-080*.

[13] Killenberg, M. (2006). *Resolution Studies of a GEM-Based TPC*. PhD thesis, Rheinisch-Westfaelische Technische Hochschule Aachen (Germany).

[14] Koufigar, S. (2015). The Radiological Footprint of a Be-based Neutron Source. Lund University devision of Nuclear Physics.

[15] Lotze, S. (2006). *Ion Backdrift Minimisation in a GEM-Based TPC Readout*. PhD thesis, Rheinisch-Westfaelische Technische Hochschule Aachen (Germany).

[16] Martin, B. R. and Shaw, G. P. (2013). *Particle physics*. John Wiley & Sons.

[17] Musa, L. (2009). Prototype compact readout system. *EUDET-Memo-2009-31, EUDET*.

[18] Olive, K. et al. (2014). Particle data group collaboration. *Chin. Phys. C*, 38:090001.

[19] Oskarsson, A. (2015-12-09). Personal communication.

[20] Sauli, F. (1977). Principles of Operation of Multiwire Proportional and Drift Chambers. *CERN Academic Training Lecture ; 81*.

[21] Tavernier, S. (2010). *Experimental techniques in nuclear and particle physics*. Springer Science & Business Media.